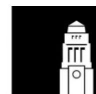

This is a repository copy of *Design of Ge/SiGe quantum-confined Stark effect modulators for CMOS compatible photonics*.

White Rose Research Online URL for this paper:
http://eprints.whiterose.ac.uk/75250/

Proceedings Paper:

Lever, L, Ikonic, Z, Valavanis, A et al. (1 more author) (2010) Design of Ge/SiGe quantum-confined Stark effect modulators for CMOS compatible photonics. In: Kubby, JA and Reed, GT, (eds.) Proceedings SPIE. Silicon Photonics V, 24 January 2010, San Francisco, California, USA. The International Society for Optical Engineering , San Francisco, California, USA , 76060Q - ? (9).

https://doi.org/10.1117/12.843223

Reuse
See Attached

Takedown
If you consider content in White Rose Research Online to be in breach of UK law, please notify us by emailing eprints@whiterose.ac.uk including the URL of the record and the reason for the withdrawal request.

eprints@whiterose.ac.uk
https://eprints.whiterose.ac.uk/

Design of Ge/SiGe quantum-confined Stark effect modulators for CMOS compatible photonics

Leon Lever, Zoran Ikonić, Alex Valavanis, and Robert W. Kelsall
University of Leeds, Woodhouse Lane, Leeds, UK

ABSTRACT

A simulation technique for modeling optical absorption in Ge/SiGe multiple quantum well (MQW) heterostructures is described, based on a combined 6×6 $\mathbf{k} \cdot \mathbf{p}$ hole wavefunction a one-band effective mass electron wavefunction calculation. Using this model, we employ strain engineering to target a specific applications-oriented wavelength, namely 1310 nm, and arrive at a design for a MQW structure to modulate light at this wavelength. The modal confinement in a proposed device is then found using finite-element modeling, and we estimate the performance of a proposed waveguide-integrated electroabsorption modulator.

1. INTRODUCTION

It is extremely desirable to develop low-cost high-volume optical transceivers for applications including interconnects, high-speed networks and fiber-to-the-home (FTTH). Silicon CMOS-based technology is a very promising candidate for such systems, owing to the highly-developed, dense level of integration. Existing carrier accumulation or depletion type Mach-Zehnder modulators are large (several millimeters in length) and dissipate considerable amounts of power.[1] As such, there exists the need to develop compact low-power modulators.

When an electric field is applied perpendicular to the plane of a a quantum well (QW), a shift in the energies of the bound states occurs.[2] This is known as the quantum-confined Stark effect (QCSE). In a type-I rectangular QW, the energies of the electron and hole ground state subbands will shift towards each other, and a red-shift of the absorption edge will be observed when the field is applied. Provided there is strong confinement, second order perturbation theory shows that the energy shift increases with the square of the applied field.

We can exploit the QCSE for electro-absorption (EA) modulation of optical signals as follows. The multiple quantum well (MQW) system is designed so that the absorption edge is close to the photon energy of the carrier. Under zero field, the absorption edge is at a larger energy than the signal, and when a field is applied the absorption edge energy is reduced so that the signal is absorbed.

The QCSE is, in principle, an extremely fast process as no injection or depletion of carriers is required, and furthermore, for the same reasons it is expected that QCSE devices should dissipate less power than carrier-depletion/accumulation devices. Modulation of the absorption coefficient of a Ge/SiGe MQW system epitaxially grown on Si wafers using reduced pressure chemical-vapor deposition (RP-CVD) has been achieved. A contrast in the absorption coefficient of a factor of 4.69 was reported, and it was proposed that this structure could be employed in an electro-absorption device operating at ~ 1450 nm.[3,4]

Of greatest commercial interest are the telecoms 'windows' at wavelengths of 1310 nm and 1550 nm. The direct bandgap of bulk Ge is 800 meV, corresponding almost exactly to 1550 nm. A strain-symmetrized MQW stack of Ge QWs and SiGe barriers will result in compressive strain of the Ge wells, which will increase the bandgap.[5,6] Choosing a high Si-fraction for the virtual substrate results in large amounts of compressive strain in the Ge QWs and allows us to shift the absorption edge to shorter wavelengths. This strain engineering approach allows us to design MQW structures for EA modulation at 1310 nm.

2. BAND STRUCTURE

To calculate the band structure of the 2D system we first consider the unstrained case. The valence band is split into three bands – light-hole (LH) and heavy-hole (HH) bands, which are degenerate at the Γ point, and a third, lower energy split-off (SO) band, which is separated by an energy ΔE_{SO} from the LH and HH bands due to spin-orbit splitting. It follows that the valence band maximum will be given by

$$E_v = \bar{E_v} + \frac{1}{3}\Delta E_{SO}, \tag{1}$$

where $\bar{E_v}$ is the average of the LH, HH and SO band edges. We can determine the shift in this energy for an epitaxial $Si_{1-x}Ge_x$ film from[7]

$$\Delta \bar{E_v} = 0.55x. \tag{2}$$

The unstrained direct bandgap was calculated by linearly interpolating between the Γ_2 gap in Si[8] and the direct gap in Ge, i.e.

$$E_g^\Gamma = 4.2(1-x) + 0.8x. \tag{3}$$

This is a good approximation, since the direct bandgap bowing in SiGe alloys is know to be weak ($\sim 0.23\,\text{eV}$).[9]

Si and Ge have a mismatch in their lattice constants, with that of Ge being 4.2% larger than in Si. Therefore, any $Si_{1-x}Ge_x$ layer lattice-matched to a relaxed $Si_{1-y}Ge_y$ substrate will exhibit compressive strain for $y > x$ and tensile strain for $x > y$. In the valence band, strain results in a splitting of the LH and HH states. This was modeled by including strain terms in the $\mathbf{k}\cdot\mathbf{p}$ Hamiltonian. The effect of strain on the conduction band edge was calculated according to model-solid theory.[10] The deformation potentials for the Ge Γ band gap in RP-CVD-grown systems described by Liu *et al.*[11] were used to calculate the modification to the band gap due to strain. This is justified because firstly Si Γ_2 strain deformation potential constants are lacking in the literature, and secondly the systems of interest have large Ge fractions, particularly in the wells where the band gap is critical to the absorption spectra.

Strain was included in the valence band by calculating the LH-HH strain splitting from $\mathbf{k}\cdot\mathbf{p}$ theory. In the conduction band, the hydrostatic strain component was found from

$$\Delta E_c^{\text{Hyd}} = a(2\varepsilon_\parallel + \varepsilon_\perp), \tag{4}$$

where $\varepsilon_\parallel$ is the in-plane strain, $\varepsilon_\perp$ is the strain perpendicular to the growth plane, and $a = -8.97\,\text{eV}$ is the hydrostatic deformation potential constant.[11] The uniaxial strain causes a shift to the conduction band edge of

$$\Delta E_c^{\text{Uni}} = 2b(\varepsilon_\perp - \varepsilon_\parallel), \tag{5}$$

where $b = -1.88\,\text{eV}$ is the uniaxial deformation potential constant.[11] The conduction band profile was therefore determined from

$$E_c = E_v + E_g^\Gamma + \Delta E_c^{\text{Hyd}} + \Delta E_c^{\text{Uni}}. \tag{6}$$

Note that here E_v is the highest energy valence band edge, which may be either HH or LH, depending on whether the strain is compressive or tensile, E_g^Γ is the unstrained direct bandgap and the uniaxial strain component, ΔE_c^{Uni}, is required despite the symmetry of the Γ-valley in order to take into account the LH–HH splitting.

Electron wavefunctions were calculated using an envelope function/one-band effective mass approximation,[12] where the effective mass in the heterostructure is found from

$$m^* = x m_{\text{Ge}} + (1-x) m_{\text{Si}}, \tag{7}$$

where $m_{\text{Ge}} = 0.042 m_0$,[13] $m_{\text{Si}} = 0.156 m_0$,[14] and m_0 is the free electron mass. Hole wavefunctions were calculated using a 6×6 $\mathbf{k}\cdot\mathbf{p}$ method,[15] and the Luttinger parameters that were used are given in Table 1.

Si	γ_1	4.22
	γ_2	0.39
	γ_3	1.44
Ge	γ_1	13.4
	γ_2	4.25
	γ_3	5.69

Table 1. Luttinger parameters used in the $\mathbf{k}\cdot\mathbf{p}$ calculation.[16]

3. OPTICAL ABSORPTION

Optical absorption was calculated according to

$$\alpha(\omega) = \alpha_{\mathrm{ex}} + C_0 \frac{2}{L}\frac{1}{4\pi}\iint \mid \mathbf{e}\cdot\mathbf{p} \mid^2 \mathrm{d}k_x \mathrm{d}k_y, \tag{8}$$

where α_{ex} is the excitonic contribution, which will be discussed later, L is the periodicity of the MQW system (i.e., the well width plus the barrier width), $\mid \mathbf{e}\cdot\mathbf{p} \mid$ is the momentum matrix element between the electron and hole wavefunctions, k_x and k_y are the wave vectors in the growth plane, the factor of two accounts for spin degeneracy, and C_0 is given by

$$C_0 = \frac{\pi e^2}{N_r c \epsilon_0 {m_0}^2 \omega}, \tag{9}$$

where ω is the angular frequency of the light and N_r is the refractive index of the material. We used a linear interpolation between Si and Ge to describe the refractive index of a material with the average composition of the MQW system.

The integration over k-space was implemented by evaluating the momentum matrix elements at a range of in-plane wavevectors and multiplying the matrix element by a normalized Lorentzian centered at the energy difference between the pair of subbands *at that point in k-space*, and multiplying by $\mathrm{d}k_x$ and $\mathrm{d}k_y$. We now have the absorption spectrum corresponding to a given pair of subbands at an (ideally infinitesimally small) finite region of the in-plane k-space. These Lorentzians were then summed to generate the resultant absorption spectra. A resolution of $\mathrm{d}k = 0.003\pi/a$, where a is the lattice constant, was used over a range of $0 < |k| < 0.06\pi/a$, and a full-width at half-maximum (FWHM) of 8 meV was used for each contribution.

The excitonic contributions to the spectra were found using a variational energy minimization approach.[17, 18] The exciton wavefunction was assumed to be of the form

$$\phi(r) = \sqrt{\frac{2}{\pi}}\frac{1}{\lambda}e^{-r/\lambda}, \tag{10}$$

where r is a parameter describing the separation of the electron and hole wavefunctions, and λ is the variational parameter (effectively the Bohr radius of the exciton). The resulting excitonic contribution to the absorption spectrum due to each pair of electron end hole subbands is then given by

$$\alpha_{\mathrm{ex}} = \frac{2C_0}{L}\mid \mathbf{e}\cdot\mathbf{p} \mid^2 \frac{2}{\pi\lambda^2}\frac{1}{\pi}\frac{\Gamma}{\left(\hbar\omega - (E_{i,j} - E_b)\right)^2 + \Gamma^2}, \tag{11}$$

where $E_{i,j}$ is the energy difference between a given pair of subband minima, E_b is the exciton binding energy, and Γ is the linewidth of the transition, which was chosen to be 8 meV in order to fit to the spectra from Kuo *et al.*[3]

4. VERIFICATION OF THE SIMULATION TECHNIQUE

In this section we will compare simulated data to the experimental data of Kuo *et al.*[3] The MQW section of that device consisted of ten periods of 10-nm-thick Ge quantum wells with 16-nm-thick $Si_{0.15}Ge_{0.85}$ barriers, and was

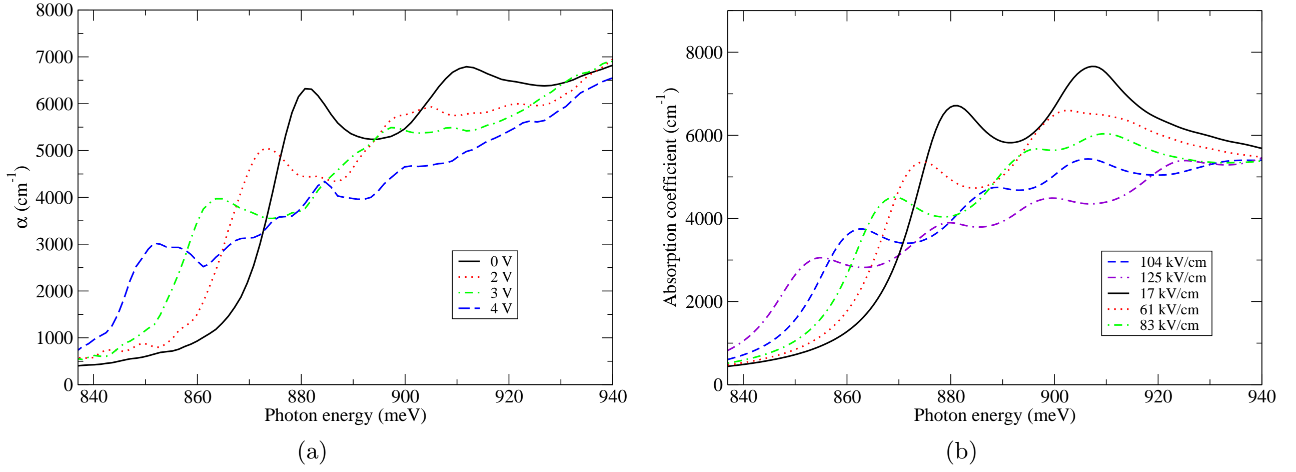

Figure 1. (a) Experimental absorption spectra using the data from Kuo *et al.*[3] (b) Simulated absorption spectra.

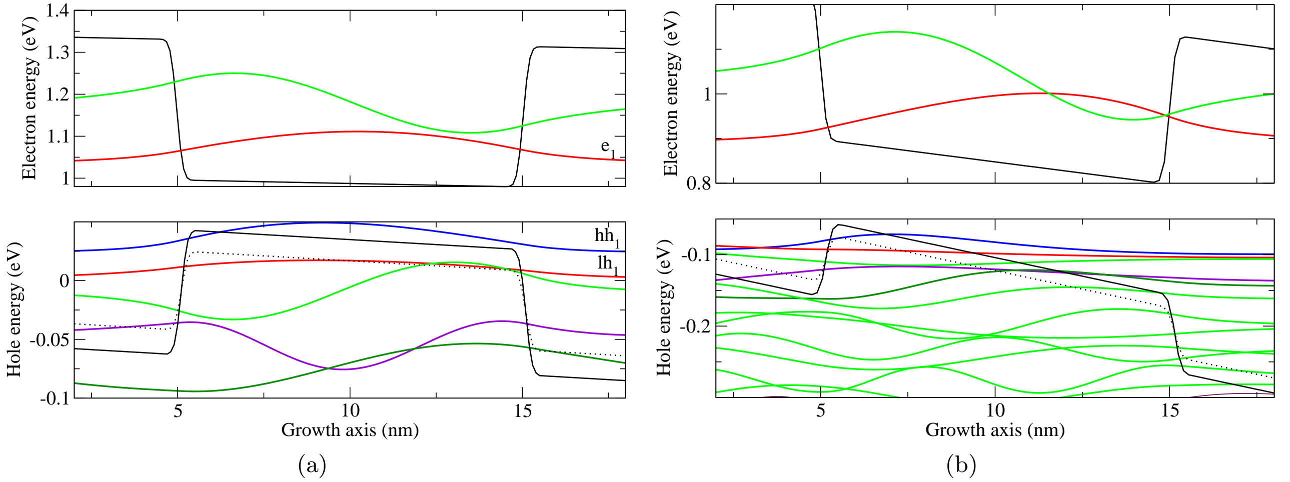

Figure 2. Band diagrams with the amplitude of the wavefunction illustrated at $k_{x,y} = 0$. The light-hole band edge is shown as the dotted line. (a) shows the the bandstructure at 17 kV/cm, with the lowest electron and hole subbands labeled, and (b) shows it at 104 kV/cm. We see that lh_1 state loses confinement at the larger field, and that additional transitions become allowed due to the loss of symmetry.

grown on a $Si_{0.1}Ge_{0.9}$ virtual substrate. A comparison of the measured absorption spectra and our simulated data is shown in figure 1.

At low fields there are two transitions that contribute to the absorption spectra shown in figure 1: $hh_1 \rightarrow e_1$ and $lh_1 \rightarrow e_1$, which give rise to excitonic peaks at 880 meV and 910 meV, respectively, where hh_i denotes the ith HH subband, lh_i the ith LH subband, and e_i is the ith electron subband. This is illustrated in the wavefunction plots shown in figure 2a, where we can see from the parity of the states that these are the only allowed transitions near to the absorption edge.

From figure 2b we can see that at larger applied fields the symmetry of the system is broken, and we find that the $hh_2 \rightarrow e_1$ and $hh_3 \rightarrow e_1$ transitions become allowed. The $lh_1 \rightarrow e_1$ transition becomes weaker as we start to lose confinement of the lh_1 state, and the peak centered at 910 meV disappears and several smaller peaks are visible as the additional transitions become allowed.

At low applied bias we find agreement in the position of the absorption edge between the simulated and experimental data. Due to the mismatch in the thermal expansion coefficients of Ge and Si, when a Ge virtual substrate is grown on a silicon wafer we find that the epitaxial Ge layer becomes tensile strained as it cools down from the growth temperature. Characterization of RP-CVD growth of Ge on Si substrates shows that this strain

is typically 0.2% (compared to the bulk lattice constant).[5,19] In this system the virtual substrate is composed of $Si_{0.1}G_{0.9}$ and is doped, and so we may expect to see some difference in the residual tensile strain. We find agreement with the position of the absorption edge by incorporating 0.1% residual strain.

We can deduce the internal field from the applied bias as follows. The device reported by Kuo *et al.*[3] consists of a p^+ contact region, on top of which is grown a 100-nm-thick intrinsic spacer layer, the 260-nm-thick MQW region, a second 100-nm-thick spacer and then an n^+ contact. If we assume that the voltage is dropped across the 460-nm-thick intrinsic region of the device, then the electric field will be given by the sum of the built-in potential due to the *p-i-n* junction, and the applied bias divided by the thickness of the intrinsic region. If we assume that the *p-n* junction bias is 0.8 V, then the internal fields will be 17, 61, 83 and 104 kV/cm for applied biases of 0, 2, 3, and 4 V, respectively. However, from the simulated spectra shown in figure 1, we find that agreement is not found using this method of determining of the internal fields. A field of 125 kV/cm is required to reproduce the shift due to an applied bias of 4 V. We attribute the discrepancy in the magnitude of the Stark shift to dopant diffusion, and find that an effective length of the intrinsic region over which the potential should be dropped in order to provide agreement with the simulated data is approximately 385 nm, which implies that the dopant diffusion from the contact layers is ~ 75 nm.

The light-hole/heavy-hole splitting is determined by the deformation potential constants given in equations 4 and 5. The splitting of the $hh_1 \rightarrow e_1$ and $lh_1 \rightarrow e_1$ excitons in the experimental spectra is approximately 30 meV. Using the deformation potential constants given by Ishikawa *et al.*[5] we find a *lh–hh* splitting of 27 meV. Prior studies simulating this system report *lh–hh* splittings of 38 meV[20] and 40 meV,[21] suggesting that the deformation potential constants determined by Ishikawa *et al.* are a better choice for the RP-CVD-grown Ge/SiGe system.

5. ELECTRO-ABSORPTION MODULATION AT 1310 NM

Many fiber-optic telecommunications systems exploit the spectral 'window' at 1310-nm. 1310 nm corresponds to zero dispersion in standard single-mode fibers, which makes it particularly suitable for EA modulation due to the greater tolerance of chirp. Passive optical network architectures typically use 1310 nm for upstream signals,[22] and so compact, low-cost and low-power modulators operating at 1310 nm that can be integrated into Si electronic-photonic integrated circuits would be extremely desirable for emerging FTTH applications.

The strain in the QWs is determined by the composition of the virtual substrate, and growing QWs on a high-Si-fraction virtual substrate will result in compressive strain in the Ge wells and hence a blue-shift of the absorption edge compared to the unstrained case. Careful choice of the composition and thickness of the barriers allows us to design an MQW structure on a strain-symmetrized substrate so that we can target 1310 nm for EA modulation.

1310 nm corresponds to a photon energy of 946 meV, and our simulated data shows that, for 8-nm Ge QWs with $Si_{0.4}Ge_{0.6}$ barriers grown on a $Si_{0.25}Ge_{0.75}$ substrate, we can expect a zero-field absorption edge at 970 meV. The larger Si fraction of the virtual substrate leads to a larger strain-splitting of the HH and LH band edges, and this is reflected in the larger separation of the simulated $hh_1 \rightarrow e1$ and $lh_1 \rightarrow e_1$ exciton peaks shown in the zero-field spectra in figure 3. Under zero field, at 946 meV the simulated absorption coefficient is 1,000 cm^{-1}; under an applied field of 220 kV/cm we see a Stark shift such that the absorption coefficient increases to 4,500 cm^{-1}.

In order to consider how this structure may perform when used as in a waveguide-integrated EA modulator, let us consider the device shown in figure 4. In that device, light couples in from an Si-rib waveguide using a tapered coupler. The waveguide considered here supports only TE-polarized light, allowing us to exploit the polarization-dependent nature of the QCSE absorption spectra. The MQW stack is biased such that the electric field is perpendicular to the growth direction, and the incoming light is vertically-coupled to the SiGe/Ge section of the device. The out-going signal then couples to a Si-rib waveguide via a second tapered waveguide adapter.

A cross-section of the MQW section of the device is shown in figure 5, with the fundamental quasi-TE mode solution calculated using Comsol Multiphysics.[23] Here, we have modeled an 8-μm-wide mesa with a 500-nm-thick *p*-type virtual substrate (consistent with Kuo *et al*'s device[3]), two 50-nm-thick spacer layers and a 100-nm-thick *n*-type top contact. A 20-well strain-symmetrized stack of QWs will have a total thickness of 300 nm, and will result in a total height of the SiGe mesa structure of 1 μm. In order to generate an applied field of 220 kV/cm in

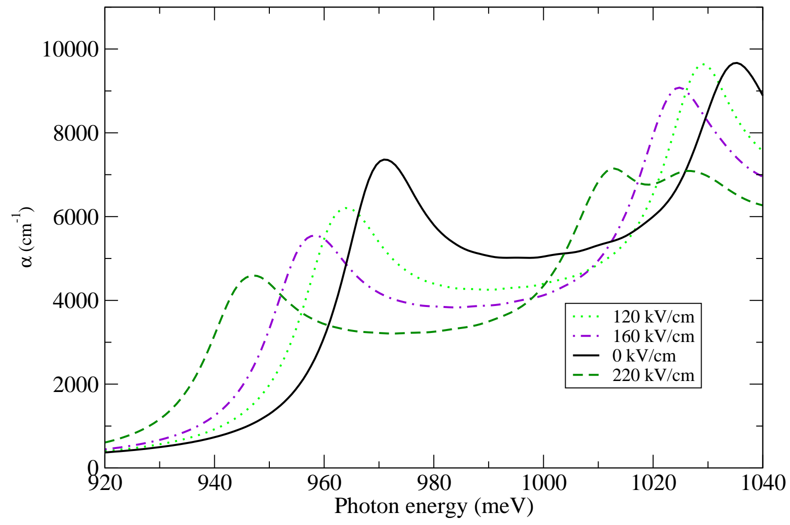

Figure 3. Simulated absorption spectra for the 1310-nm EA MQW structure.

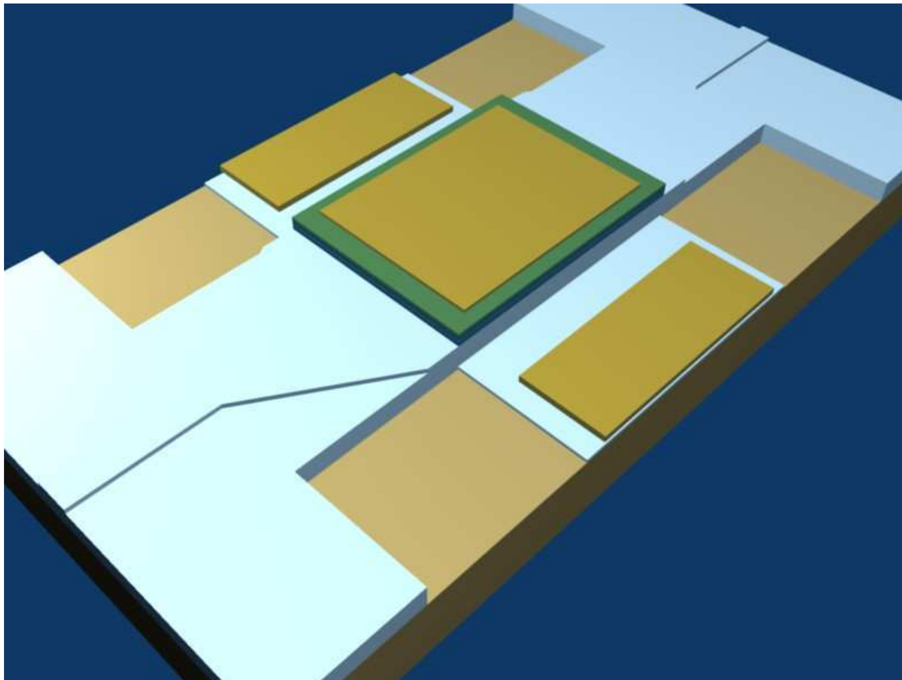
Figure 4. Illustration of the proposed waveguide-integrated QCSE device.

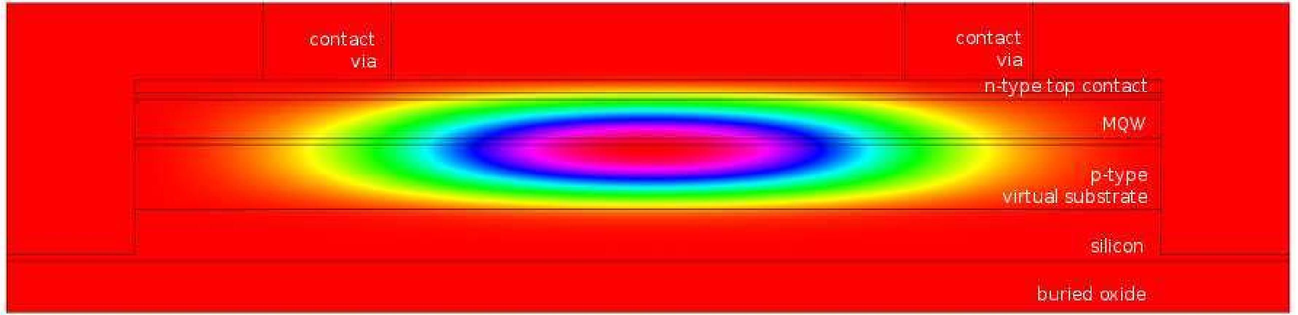

Figure 5. 8-μm-wide mesa cross-section. The power density of the fundamental TE mode is shown in a pseudo-color plot. The metal contact vias are displaced from the centre of the mesa; this improves the modal overlap with the MQW section and reduces the losses compared to a metallisation layer that covers the whole top surface.

the MQW region of the device, an applied bias of 5.5 V is required.* The finite element method (FEM) modeling shows that we can expect a modal overlap with the optically active MQW section of the device of 30%. This figure can be improved by making the virtual substrate thinner – for example, a 200-nm-thick virtual substrate leads to a modal overlap of 54%.

Using the absorption coefficients in the on- and off-states of the MQW structure, together with the modal overlap, we can estimate the performance of the device. Assuming no coupling loss, and that absorption only occurs in the MQW region, the extinction ratio and insertion loss are plotted in figure 6 as a function of the length of the device. We find that for a 25-μm-long device, an extinction ratio of 11 dB is expected with an insertion loss of 3 dB.

In order to improve these estimates, we have simulated propagation using a hybrid mode in-plane propagation model, where the complex part of the refractive index in the MQW section of the device is determined using the simulated absorption coefficients at 1310 nm. TE radiation was launched into the device using the predefined port boundary conditions, and the attenuation of the signal determined from the S-parameters. For a 43-μm-long device we find an insertion loss of 4 dB and an extinction ratio of 11 dB. The additional insertion loss arises due mainly to reflections at the start and end of the mesa, and the reduced extinction ratio results from the non-ideal coupling of the incoming waveguide mode to the fundamental mode in the device.

6. CONCLUSIONS

We have developed a computational tool for modeling the absorption spectra in Ge/SiGe multiple quantum well heterostructures. The model is based on a 6×6 $\mathbf{k} \cdot \mathbf{p}$ hole wavefunction calculation and a one-band effective mass model for electrons, and includes the effects of strain and excitons. We find that we are able to accurately reproduce the relevant experimental data with minimal fitting of parameters.

This simulation technique was used to design an MQW structure to target 1310-nm light by engineering the strain in the virtual substrate. Our simulated data shows that we can expect a contrast in the absorption coefficient of a factor of 4.5 at this wavelength. FEM modeling of proposed waveguide-integrated device designs shows that we can expect compact (less than 50-μm-long) devices with an insertion loss of 4 dB, extinction ratio of 11 dB and an operating bias of ~ 5 V.

REFERENCES

[1] Liu, J., Beals, M., Pomerene, A., Bernardis, S., Sun, R., Cheng, J., Kimerling, L. C., and Michel, J., "Waveguide-integrated, ultralow-energy GeSi electro-absorption modulators," *Nature Photonics* **2**(7), 433–437 (2008).

*As we have seen in the simulations of Kuo *et al.*'s device, we may expect some ingress of dopants into the nominally intrinsic spacer layers, and so this may be an over-estimate of the required voltage.

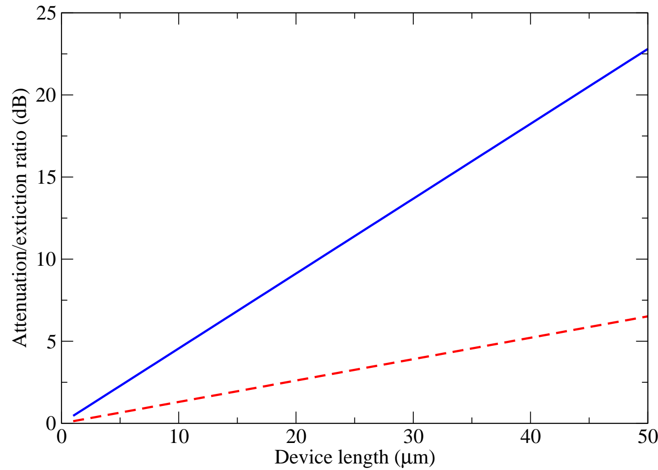

Figure 6. The dashed line shows the insertion loss, and the solid line shows the extinction ratio.

[2] Miller, D. A. B., Chemla, D. S., Damen, T. C., Gossard, A. C., Wiegmann, W., Wood, T. H., and Burrus, C. A., "Band-edge electroabsorption in quantum well structures: The quantum-confined Stark effect," *Physical Review Letters* **53**, 2173–2176 (Nov 1984).

[3] Kuo, Y.-H., Lee, Y. K., Ge, Y., Ren, S., Roth, J. E., Kamins, T. I., Miller, D. A. B., and Harris, J. S., "Strong quantum-confined Stark effect in germanium quantum-well structures on silicon," *Nature* **437**, 1334–1336 (2005).

[4] Kuo, Y.-H., Lee, Y. K., Ge, Y., Ren, S., Roth, J. E., Kamins, T. I., Miller, D. A. B., and Harris, J. S., "Quantum-confined stark effect in Ge/SiGe quantum wells on Si for optical modulators," *IEEE Journal of selected topics in quantum electronics* **12**, 1503–1513 (2006).

[5] Ishikawa, Y., Wada, K., Liu, J., Cannon, D. D., Luan, H.-C., Michel, J., and Kimerling, L. C., "Strain-induced enhancement of near-infrared absorption in Ge epitaxial layers grown on Si substrate," *Journal of Applied Physics* **98**(1), 013501 (2005).

[6] Paul, D. J., "Si/SiGe heterostructures: from material and physics to devices and circuits," *Semiconductor Science and Technology* **19**, R75R108 (2004).

[7] Afanas'ev, V. V., Stesmans, A., Souriau, L., Loo, R., and Meuris, M., "Valence band energy in confined $Si_{1-x}Ge_x$ ($0.28 < x < 0.93$) layers," *Applied Physics Letters* **94**(17), 172106 (2009).

[8] "NSM archive – physical properties of semiconductors." www.ioffe.rssi.ru/SVA/NSM/Semicond.

[9] Tekia, F., Ferhat, M., and Zaoui, A., "Band-gap bowing in Si_xGe_{1-x} alloy," *Physica B: Condensed Matter* **293**(1-2), 183–186 (2000).

[10] Van de Walle, C. G., "Band lineups and deformation potentials in the model-solid theory," *Physical Review B* **39**, 1871–1883 (Jan 1989).

[11] Liu, J., Cannon, D. D., Wada, K., Ishikawa, Y., Danielson, D. T., Jongthammanurak, S., Michel, J., and Kimerling, L. C., "Deformation potential constants of biaxially tensile stressed Ge epitaxial films on Si(100)," *Phys. Rev. B* **70**, 155309 (Oct 2004).

[12] Valavanis, A., Lever, L., Evans, C. A., Ikonic, Z., and Kelsall, R. W., "Theory and design of quantum cascade lasers in (111) n-type Si/SiGe," *Physical Review B* **78**(3), 035420 (2008).

[13] Fischetti, M., "Monte Carlo simulation of transport in technologically significant semiconductors of the diamond and zinc-blende structures. I. Homogeneous transport," *Electron Devices, IEEE Transactions on* **38**, 634–649 (Mar 1991).

[14] Cardona, M. and Pollak, F. H., "Energy-band structure of germanium and silicon: the $\mathbf{k}\cdot\mathbf{p}$ method," *Physical Review* **142**(2), 530–543 (1966).

[15] Harrison, P., [*Quantum Wells, Wires and Dots: Theoretical and Computational Physics of Semiconductor Nanostructures*], Wiley, Chichester, 2nd ed. (2005).

[16] Kahan, M., Chi, M., and Friedman, L., "Infrared transitions in strained-layer Ge_xSi_{1-x}/Si," *Journal of Applied Physics* **75**, 8012–8021 (1994).

[17] Fox, A. M., Miller, D. A. B., Livescu, G., Cunningham, J. E., and Jan, W. Y., "Excitonic effects in coupled quantum wells," *Physical Review B* **44**, 6231–6242 (Sep 1991).

[18] Susa, N., "Improvement in electroabsorption and the effects of parameter variations in the three-step asymmetric coupled quantum well," *Journal of Applied Physics* **73**(2), 932–942 (1993).

[19] Rouviere, M., Halbwax, M., Cercus, J.-L., Cassan, E., Vivien, L., Pascal, D., Heitzmann, M., Hartmann, J.-M., and Laval, S., "Integration of germanium waveguide photodetectors for intrachip optical interconnects," *Optical Engineering* **44**, 075402 (2005).

[20] Virgilio, M. and Grosso, G., "Quantum-confined stark effect in Ge/SiGe quantum wells: A tight-binding description," *Physical Review B (Condensed Matter and Materials Physics)* **77**(16), 165315 (2008).

[21] Paul, D. J., "8-band $\mathbf{k}\cdot\mathbf{p}$ modeling of the quantum confined stark effect in ge quantum wells on si substrates," *Physical Review B (Condensed Matter and Materials Physics)* **77**(15), 155323 (2008).

[22] Lam, C., [*Passive Optical Networks Principles and Practice*], Elsevier (2007).

[23] "Comsol multiphysics." www.comsol.com.